On the application of laser shock peening for retardation of surface fatigue cracks in laser beam-welded AA6056

Kashaev, Nikolai; Ushmaev, Dmitrii; Ventzke, Volker; Klusemann, Benjamin; Fomin, Fedor

Published in:
Fatigue and Fracture of Engineering Materials and Structures

DOI:
10.1111/ffe.13226

Publication date:
2020

Document Version
Publisher's PDF, also known as Version of record

Received: 22 December 2019 | Revised: 13 March 2020 | Accepted: 21 March 2020

DOI: 10.1111/ffe.13226

ORIGINAL CONTRIBUTION

FFEMS Fatigue & Fracture of Engineering Materials & Structures WILEY

On the application of laser shock peening for retardation of surface fatigue cracks in laser beam-welded AA6056

Nikolai Kashaev[1] | **Dmitrii Ushmaev**[1] | **Volker Ventzke**[1] | **Benjamin Klusemann**[1,2] | **Fedor Fomin**[1]

[1]Institute of Materials Research, Materials Mechanics, Helmholtz-Zentrum Geesthacht, Max-Planck-Str. 1, D-21502, Geesthacht, Germany

[2]Institute of Product and Process Innovation, Leuphana University of Lüneburg, Universitätsallee 1, D-21335, Lüneburg, Germany

Correspondence
Nikolai Kashaev, Institute of Materials Research, Materials Mechanics, Helmholtz-Zentrum Geesthacht, Max-Planck-Str. 1, D-21502 Geesthacht, Germany.
Email: nikolai.kashaev@hzg.de

Abstract

The present study aims to investigate the extent to which the fatigue behaviour of laser beam-welded AA6056-T6 butt joints with an already existing crack can be improved through the application of laser shock peening. Ultrasonic testing was utilized for in situ (nondestructive) measurement of fatigue crack growth during the fatigue test. This procedure allowed the preparation of welded specimens with surface fatigue cracks with a depth of approximately 1.2 mm. The precracked specimens showed a 20% reduction in the fatigue limit compared with specimens without cracks in the as-welded condition. Through the application of laser shock peening on the surfaces of the precracked specimens, it was possible to recover the fatigue life to the level of the specimens tested in the as-welded condition. The results of this study show that laser shock peening is a very promising technique to recover the fatigue life of welded joints with surface cracks, which can be detected by nondestructive testing.

KEYWORDS

aluminium alloys, fatigue crack, laser beam welding, laser shock peening, residual stress, ultrasonic crack tip diffraction

1 | INTRODUCTION

As an efficient joining technology, laser beam welding (LBW) is already established for lower fuselage applications in Airbus aircrafts.[1–3] The welding process is industrially realized at large-scale LBW facilities equipped with two CO_2 lasers for simultaneous double-sided welding of the long-distance T-joints (skin–stringer joints) of 6xxx series Al-alloys (Al–Mg–Si). Laser beam-welded structures show a better buckling behaviour under compression loading compared with riveted structures.[3] However, the application of LBW is limited to structures experiencing compressive loading conditions, as laser beam-welded joints show an inferior damage tolerance behaviour under tension loading compared with riveted structures.[3]

The damage-tolerance-design philosophy applied for aircraft structures considers possible initiating of fatigue cracks where the propagation of the initiated cracks must be significantly retarded by appropriate design concepts so as to detect any crack of a critical length during the scheduled inspections.[4–6] The propagation of fatigue cracks is quite different in welded and riveted structures.[3] In a riveted structure, a skin crack propagates towards a

stringer without penetrating through the stringer. Therefore, the stringer remains undamaged and reduces the stress concentration at the crack tip by bearing a part of the applied load. In contrast, a skin crack in welded structures propagates towards a stringer where it branches into several cracks, with one crack tip growing vertically into the stringer. When the stringer fails, its stress-bridging effect is lost, leading to premature failure of the whole structure.[3]

One way to improve the fatigue performance of integral welded structures is the introduction of so-called crack retarders or crack stoppers. The mechanisms and usage of crack stopper straps as an effective approach to increase the damage tolerance of fuselage structures were described by Liebowitz.[7] When a crack grows in an aluminium structure and the crack tip reaches the position of a crack retarder, the crack retarder partly carries the external load. Hence, the stress concentration at the crack tip is lowered and the crack growth rate is reduced. In case of Airbus A380, titanium crack stoppers are installed between the skin and stringers in critical areas; they are always riveted because a bonding process is not available with the required reliability with regard to corrosion and durability.[8] Zhang et al. have investigated the effectiveness of crack growth retarders from carbon fibre-reinforced polymer, glass fibre-reinforced polymer and titanium alloy Ti–6V–4Al bonded to aluminium alloys 2024-T351 and 7085-T7651.[9] A retardation effect was observed for all material configurations, but it was more significant when the straps were behind the propagating crack tip. A high strength Ti–6Al–4V alloy strap was identified as the most effective material for crack retarders.

Another promising fatigue crack retardation concept is crenellation, where the thickness of the fuselage skin is systematically varied whereas the structural weight remains unchanged. The systematic thickness variation modulates the stress-intensity factor profile and retards fatigue crack growth.[10] The effectiveness of the crenellation concept can still be increased if it is combined with beneficial residual stresses introduced through a laser-heating process.[11] Laser-heating techniques utilize the widely spread compressive residual stress field surrounding the heating line to retard the growth of long fatigue cracks.[12] Compressive residual stresses can also be introduced through overloading,[13–15] indentation[16–18] and cold expansion.[19,20] One of the easiest methods to reduce the stress concentration at the crack tip to retard fatigue crack growth in already cracked structures is to drill a hole to the crack tip. The effectiveness of the stop-drilling technique on fatigue crack growth retardation or even on fatigue crack arrest has also been extensively studied over the years.[21–23]

To avoid stringer failure and therefore to improve the damage-tolerance behaviour of welded structures, the initiation of possible fatigue cracks and the propagation of already initiated cracks should be prohibited. In case of laser beam welding of aluminium alloys, the fatigue critical zones are in the weld (or at the heat-affected zone/fusion zone of the weld boundary). Here, the crack can be initiated due to possible welding defects like the existence of pores due to reduced strength compared with the base material—this can be attributed to precipitation dissolution in case of some aluminium alloys as well as to the introduced tensile residual stresses. A promising way to improve the fatigue behaviour of welds is to introduce compressive residual stresses, whereby laser shock peening (LSP) could be seen an effective residual stress engineering method to generate deep compressive residual stress fields in metallic materials.[24–26]

The principle of the LSP process can be described as follows: see, for example, Montross et al.[24] For LSP treatment of the material surface, which is usually covered by a water-confirming layer, a laser beam with high-pulse energy is used. Having passed through water, the laser beam is absorbed by the material, which turns into plasma. Subsequently, the plasma expands very rapidly by absorbing the laser energy during the pulse. The transparent water layer traps the plasma, thereby causing a higher pressure at the material surface. The energy of the high-pressure plasma partially turns into mechanical shock waves within the material. Plastic material deformation occurs when the shock wave pressure exceeds the dynamic yield strength, which, in turn, leads to compressive residual stresses below the treated area and balancing tensile residual stresses in the surrounding areas.

LSP treatment has a strong beneficial effect on the fatigue performance of structural components because the compressive residual stress field induced in the material considerably retards fatigue crack growth.[27–34] Therefore, a significant improvement in the fatigue behaviour and lifetime prolongation can be achieved for components and structures with surface cracks[27,28,31,34] as well as through-thickness cracks.[29,30,32,33] Lin et al. have investigated the effect of LSP on the fatigue strength of engine components subjected to foreign object damage (FOD), where LSP is applied before FOD.[35] A delayed crack onset and reduced early fatigue crack growth rates for Ti–6Al–4V specimens with LSP treatment compared with specimens without LSP treatment are reported. Luo et al. have shown the recovery of the fatigue life of Ti–6Al–4V specimens subjected to FOD by the application of LSP.[36] The positive effect of the LSP-induced compressive residual stresses was found in the reduction of stress values in the FOD area. However, most of the previous

research works investigated the effect of LSP-induced compressive residual stresses on long through-thickness cracks. There is still a lack of understanding when it comes to the behaviour of surface cracks within the residual stress field induced by LSP. Because the LSP process enables the generation of relatively deep residual stresses, this can potentially affect the growth of surface cracks. The conventional shot peening process does not provide these benefits due to a significantly lower penetration depth of the residual stresses.

Damage can also be introduced during the maintenance of aircraft structures. A typical example is scribe marks at fuselage joints: these might be introduced on the fuselage skin along longitudinal and circumferential joints due to the use of sharp tools during the sealant removal process prior repainting. Cini and Irving have reported a fatigue life reduction of up to 97.8% due to the presence of scribe marks in AA2024-T351 aluminium specimens under tensile and bending loads.[37] Smyth et al. have shown that LSP is also a promising technique to recover the fatigue life of AA2024-T351 aluminium specimens containing scratch damage.[38] The authors have presented that the peening of the area containing a scribe mark increases the fatigue life, depending on the specific residual stress field. However, the study also shows that LSP treatment does not influence the initiation of cracks at scribe roots.

The above-mentioned examples confirm the promising potential of LSP as a technique to improve the resistance to impact damage or to repair already existing damage in jet engine parts and aircraft structures. This study aims to improve the fatigue performance of laser beam-welded aluminium aircraft structures by suppressing any possible crack initiation and/or further crack growth in the welds. The objective of the present paper is to prove that LSP can be successfully implemented to recover the fatigue life of laser beam-welded specimens with already existed fatigue cracks. Additionally, a way to use the ultrasonic technique as a nondestructive testing for measuring the fatigue crack depth has been presented.

2 | MATERIALS AND EXPERIMENTAL PROCEDURES

2.1 | Materials and laser beam welding

As a fusion-weldable aluminium alloy, the precipitation-hardened Al–Mg–Si–Cu alloy AA6056 is used by the Airbus company as the skin material for manufacturing fuselage structures by LBW.[3] Compared with the widely used AA2024 in aircraft airframes, AA6056 does not show significant challenges for LBW regarding hot cracking susceptibility that can be avoided by the application of an appropriate aluminium filler wire material with a high Si content.[39] In this study, the AA6056 sheet material with a thickness of 6.2 mm was cut into blanks (250-mm width and 500-mm length). The sheets were peak aged at 190°C for 4 h to T6 heat treatment condition before LBW. The blanks were milled and cleaned, vacuum clamped and laser beam-welded in butt joint configurations with two 3.5-kW CO_2 lasers using the dual LBW technique and the Si-rich aluminium alloy AA4047 as a filler wire material. A laser power of 2×3.25 kW and an advance speed of 2.0 m/min were used during the welding. The inert gas Ar was used as the shielding gas. The final welded coupons were 500 mm wide and 500 mm long with the weld at the centre. The welding direction corresponds to the rolling direction of the sheet material.

The microstructure of the specimens was analysed by optical microscopy. For this purpose, the laser beam-welded butt joint was grinded in several stages; it was also polished and etched using Keller's reagent in the final preparation step. The surfaces of the fractured specimens were investigated using the stereomicroscope and the scanning electron microscope (SEM).

A typical cross-section of the resulting butt joint, showing the typical 'V' shape of the weld, is illustrated in Figure 1. Further details regarding the LBW process can be found in previous studies.[40,41] Singe round-shaped pores are frequently observed in the fusion zone (FZ) (see Figure 1A). The porosity is a common problem in the fusion welding of the aluminium alloys of the 6xxx series.[42] No indications on solidification cracking or liquidation cracking in FZ or in the heat-affected zone (HAZ) can be observed in the current work. The FZ of the weld shows a fine-grained dendritic microstructure with Si-, Cu- and Mg-rich precipitates at the grain boundaries (Figure 1B).[40]

2.2 | Mechanical characterization

The load-controlled axial fatigue tests at room temperature were conducted at a Testronic 100-kN RUMUL resonant testing machine. The tests were performed in accordance with the ASTM E466-07 standard[43] at a frequency of around 90 Hz and an applied load ratio of $R_F = 0.1$. The geometry of the specimens extracted from the laser beam-welded plates is shown in Figure 2A. The specimens for the fatigue test have a uniform test section of 15-mm width and 30-mm length. The welding seam is at the centre of the gauge length. The cyclic loading was applied transverse to the weld direction. In case

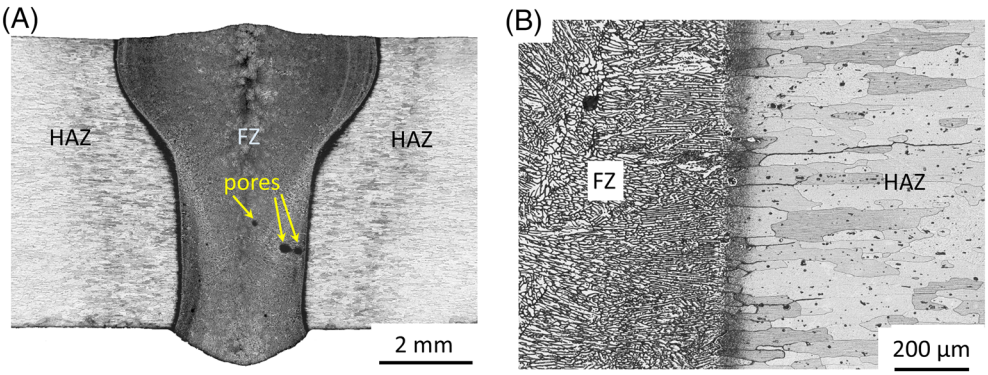

FIGURE 1 (A) Optical macrograph of a representative cross-section of a laser beam-welded butt joint. The typical 'V' shape of the weld as well as some single round-shaped pores can be seen. (B) Detailed view of the FZ/HAZ region [Colour figure can be viewed at wileyonlinelibrary.com]

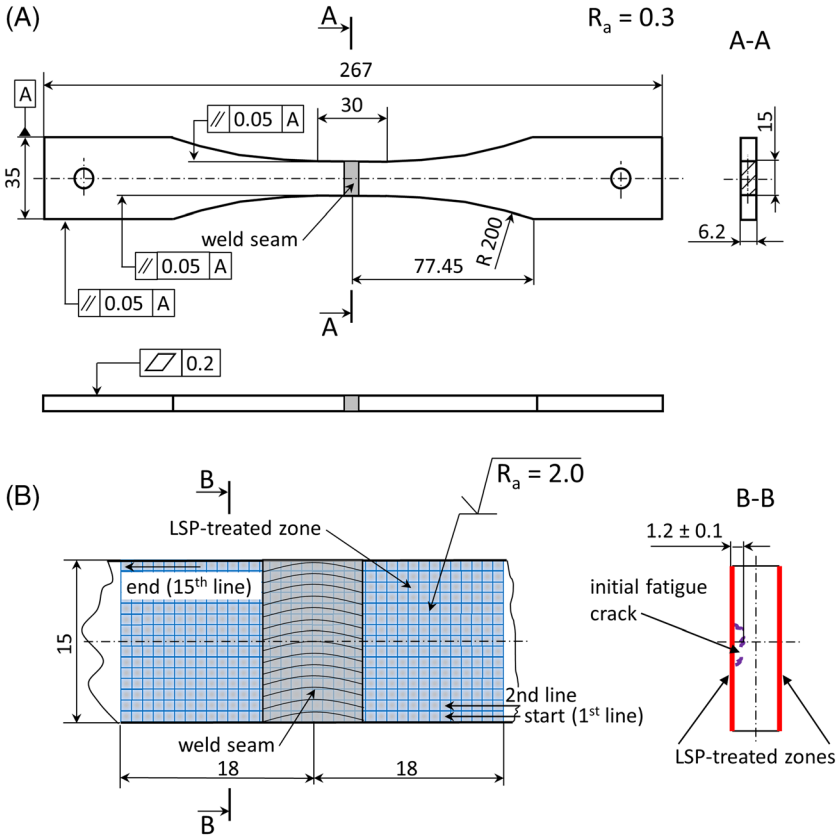

FIGURE 2 (A) Geometry of the fatigue test specimens including the weld at the centre of the specimen. (B) Schematic view of the LSP-treated region. All dimensions are in millimetre [Colour figure can be viewed at wileyonlinelibrary.com]

of LSP-treated specimens, LSP treatment was applied on both sides in accordance with the shot pattern shown in Figure 2B—only one layer of the treatment was applied without any overlap. The treated area covers the full welding seam and the neighbouring region, up to 18 mm from the centre line (see Figure 2B).

2.3 | Ultrasonic testing

Subjected to cyclic loading, the laser-welded AA6056 butt joints exhibit surface crack initiation in the weld zone. After the initiation phase, fatigue cracks are propagating perpendicular to the applied stress—that is, in the thickness direction. The crack depth as a function of the number of cycles is very important for optimizing the application of LSP treatment. Therefore, the crack depth is carefully determined during the fatigue test through ultrasonic testing based on the pulse-echo method. Fatigue and ultrasonic testing have been performed simultaneously to determine the initiation time of crack formation and to measure crack growth at a specified load and resonant frequency. The phased array technique using an ultrasonic apparatus (Olympus OmniScan MX2) was applied, whereby the ultrasonic waves were introduced obliquely into the specimen at a certain angle. The formation and propagation of a crack change the acoustic properties and

hence a part of the transmitted ultrasonic waves is reflected at the crack tip, subsequently receiving the ultrasonic probe. The measured time difference between the transmitted and reflected ultrasonic waves enables the localization of the crack tip and the determination of the crack depth. To measure the crack depth, the crack tip diffraction technique was employed. To locate the crack tip and subsequently to measure the crack depth, a spherical wave front diffracted from the sharp crack tip was used. The application of the crack tip diffraction method, which is a type of backscatter sizing techniques for the size determination of internal flaws in the material, has been described in detail by Jacques et al.[44] The principle of the application of the ultrasonic-phased array technique for measuring the fatigue crack depth is schematically shown in Figure 3. The frequency and size of the linear-phased array ultrasonic probe were 10 MHz and 4.96 mm × 5.00 mm, respectively. The angle of the wedge was 45° to propagate the ultrasonic waves in the direction between 40° and 80°.

For in situ fatigue crack growth measurement during the fatigue test, the ultrasonic technique was calibrated on specimens fabricated from the investigated alloy with mechanically introduced notches of 0.5, 1.0, 2.0 and 2.5 mm in depth that should imitate the semielliptical crack growth from the surface. Additional validation of the crack measurement technique was performed using nonfailed specimens. In this case, the fatigue crack depth was measured using ultrasonic testing and validated by cutting the specimens and measuring the crack depth, as shown for the fatigue crack (see cross section) in Figure 4. These results are in good agreement with each other, validating the ultrasonic testing procedure. The typical diagram of an ultrasonic signal for a specimen with a fatigue crack is shown in Figure 4. The fatigue crack depth was measured as a distance between the centres of the corner signal and the crack tip signal. The method's accuracy was estimated as ±0.1 mm on mechanically induced calibration notches. It should be mentioned that the crack depth measured by this technique has an averaging effect, which means that an 'effective' surface crack depth through the entire specimen thickness is determined. For more precise measurement of the short cracks, a potential drop technique might be used.[45]

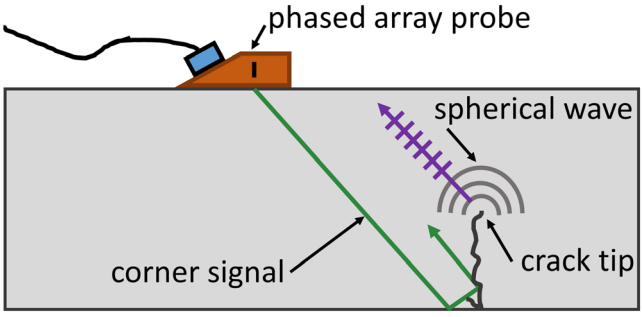

FIGURE 3 Schematic representation of ultrasonic-phased array technique for the measurement of the fatigue crack depth [Colour figure can be viewed at wileyonlinelibrary.com]

2.4 | Laser shock peening

LSP was performed using a Q-switched Nd:YAG laser operating at 10 Hz with a wavelength of 1064 nm and a pulse duration of 20 ns (FWHM). A diffractive optical element was used to deliver 5 J to the square spot of 1 mm × 1 mm on a specimen surface covered with a steel foil. LSP was applied to the fatigue specimens with surface cracks on both specimen surfaces, as shown in Figure 2B. LSP treatment on the opposite side of a specimen with a crack has basically a negative impact on the residual stress state in the middle of the specimen. However, this procedure minimizes the specimen distortion that is critical for further fatigue testing.

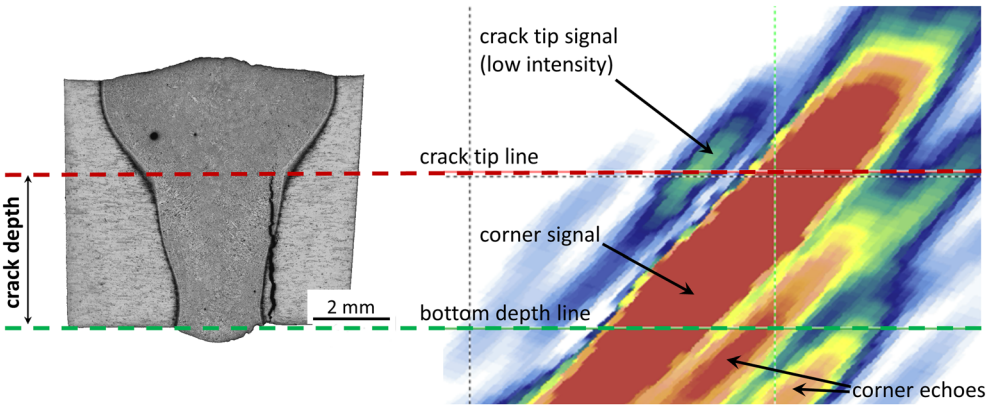

FIGURE 4 Typical diagram of ultrasonic testing (S-scan). It shows a typical signal of a measurement performed for a cracked specimen tested at 130 MPa and stopped at approximately 4×10^5 cycles. The cross-section of the specimen was extracted after ultrasonic testing and represented together with the ultrasonic signal diagram [Colour figure can be viewed at wileyonlinelibrary.com]

3 | RESULTS AND DISCUSSION

3.1 | Fatigue-testing of specimens in as-welded condition and preparation of specimens with surface fatigue cracks

To estimate the fatigue behaviour of specimens with welds, the first set of specimens with butt joints were tested at maximum cyclic stress levels between 90 and 200 MPa. The results are shown in Figure 5 (black filled squares). During the fatigue test, the resonant frequency was recorded as a function of the current number of cycles. An exemplary resonant frequency result for the specimen tested at 130 MPa is displayed in Figure 5 (red continuous line). In this representative example, the resonant frequency continuously increased during the test up to a number of cycles of approximately 2.2×10^5, followed by a decrease until the specimen broke at approximately 4.1×10^5 cycles. According to similar observations by Lorenzino and Navarro during fatigue tests,[46] the increasing resonant frequency can indicate an increase in the specimen stiffness due to cyclic hardening during the fatigue test. The decrease in the resonant frequency relates to a decrease in the specimen stiffness owing to the increased fatigue crack depth as well as the unstable rupture of the specimen connected with a rapid decrease in the resonant frequency. The results suggest that the fatigue crack could be initiated during the fatigue test in a period of up to approximately 2.2×10^5 cycles, and then, the fatigue crack was growing slowly in the period of cycles between approximately 2.2×10^5 and approximately 3.5×10^5. In addition, after approximately 3.5×10^5 cycles, the crack reached a critical depth and flowed into an unstable rupture of the specimen due to a significant reduction in the load-bearing specimen thickness.

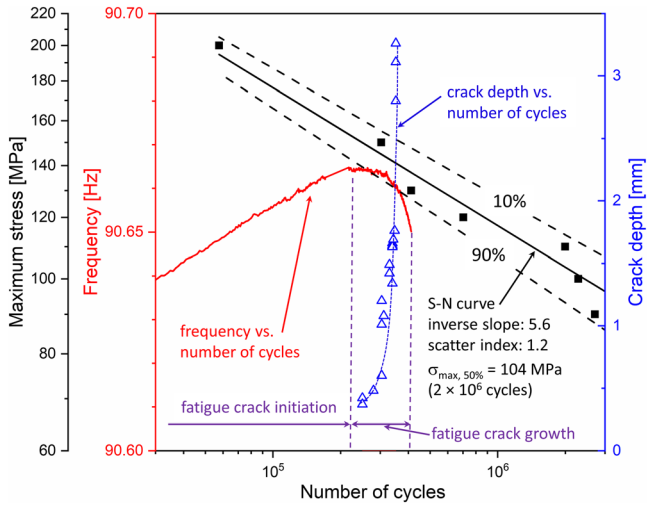

FIGURE 5 Fatigue test results of specimens in the as-welded condition (black filled squares); resonant frequency vs. number of cycles record obtained during the fatigue test of the specimen tested at 130 MPa (red curve). The fatigue test at the maximum cyclic stress level of 130 MPa was interrupted at each 5000 cycles during the test in the fatigue crack growth regime (number of cycles between 2.5×10^5 to 3.5×10^5) to measure the crack depth using ultrasonic testing (blue triangles) [Colour figure can be viewed at wileyonlinelibrary.com]

Figure 6A shows the cross-section of a specimen tested at a maximum stress of 130 MPa. The test was stopped close to the point where a rapid decrease in resonant frequency should follow. In the cross section, there is a fatigue crack that was initiated at the weld root side close to the FZ/HAZ boundary and propagated through the specimen thickness up to a depth of approximately 3.9 mm transverse to the loading direction of the specimen. In Figure 6B, a macrograph of the fractured specimen surface is shown, where two regions can be identified. In the first region, visible in the bottom part, a stable fatigue crack growth was present. The semielliptical crack, initiated from the surface, was growing up to a critical depth of approximately 3.2 mm. After reaching this critical depth, an unstable crack growth occurred, representing the second region, followed by the final rupture of the specimen. A stable fatigue crack growth could be seen in 37% of the total crack area. An ellipse with an aspect ratio of approximately 2:1 shows that the shape is partially close to the boundary between both stable and unstable fatigue crack growth. These results indicate that in case of welding joints, semielliptical crack growth from the weld root side is typically present due to the application of cyclic loading. As the geometrical quantity to evaluate the crack size, the maximum fatigue crack depth in the central region of the specimen section is considered.

For the preparation of specimens with surface fatigue cracks, an additional fatigue test at the maximum stress level of 130 MPa was performed. Between 2.5×10^5 and 3.5×10^5 cycles, the fatigue test was stopped in intervals of 5000 cycles to measure the fatigue crack depth using the calibrated ultrasonic technique. The results of the crack growth measurement during the fatigue test are presented in Figure 5 (blue triangles). It is interesting to note that the growth of the fatigue crack depth is in good agreement with the decrease in resonant (natural) frequency f_0 (Figure 5, red curve), which can be described as a function of system stiffness k and mass m:

$$f_0 = \frac{1}{2\pi}\sqrt{\frac{k}{m}}. \quad (1)$$

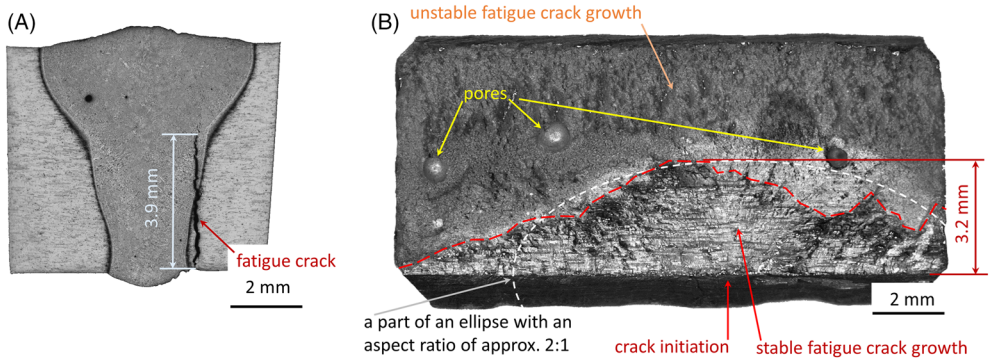

FIGURE 6 (A) Cross-section of a specimen during the fatigue test before failure. The test was conducted at 130 MPa and stopped at approximately 4×10^5 cycles. The maximum depth of the semielliptical fatigue crack measured in the cross-section is 3.9 mm. (B) Macrograph of the fractured surface of the specimen tested at 110 MPa, approximately 2.00×10^6 cycles. A stable fatigue crack growth is seen in approximately 37% of the total crack area. The part of an ellipse with an aspect ratio of approximately 2:1 shows that the shape is partially close to the boundary between both stable and unstable fatigue crack growth [Colour figure can be viewed at wileyonlinelibrary.com]

A steep decrease in the resonant frequency can be correlated with the growth of a crack, reducing the total stiffness of the system according to

$$k_\Sigma = \frac{k_m k_s}{k_m + k_s}, \tag{2}$$

where k_m is the stiffness of the machine and k_s is the stiffness of the specimen in case of axial load. The stiffness of the specimen, approximating it as a tensile bar, can be calculated as

$$k_s = \frac{AE}{L}, \tag{3}$$

where E is the elastic modulus of the specimen and L is length of the specimen with an uniform cross-section A. Linear growth of the natural frequency during the initial stages of the fatigue test might be a result of work hardening of the material, whereas a drop in the natural frequency is associated with a developing crack.

To study the effect of LSP on the naturally initiated fatigue cracks, specimens with a predefined crack depth were produced. One specific crack depth was chosen as a compromise between the inspection capability and the critical crack depth. Based on the previous fatigue test results, a reasonable crack depth (more than 0.5 mm) and at the same time less than the critical depth (~2.9 mm) leading to an unstable crack growth is targeted. Therefore, the fatigue crack depth of 1.2 mm was considered in this study for the following investigation.

To produce the required number of the specimens—that is, 10 specimens in the current study—fatigue tests were performed at 130 MPa. Starting from 2.0×10^5 cycles, the crack depth has been regularly (each 5000 cycles) inspected using ultrasonic testing. As soon as the crack reached the targeted depth of 1.2 mm, the specimen was removed.

3.2 | Introducing LSP-induced compressive residual stresses in the volume with fatigue crack

LSP is an effective process for generating deep compressive residual stresses in metallic materials up to a depth of several millimetres.[26] Compressive LSP-induced residual stresses have a positive effect on the retardation of fatigue crack propagation. The positive retardation effect of LSP treatment on the propagation of long cracks in fatigue crack propagation was successfully demonstrated in the study of Hatamleh et al.[47] The aim of the application of LSP in the current study was to introduce compressive residual stresses in specimens with surface fatigue cracks with a depth of 1.2 mm to recover the fatigue life of the precracked specimens. It means that the compressive residual stresses have to be introduced up a specimen depth of more than 1.2 mm. Based on previous process optimization of LSP for the aluminium alloy AA2024,[48] the energy of the laser was set at its maximum value of 5 J and the smallest spot size was choosen to generate the highest energy density possible with the available equipment at the specimen surface. Additionally, a steel foil is used throughout this study. To illustrate the effect of these LSP parameters on the residual stress distribution, base material specimens of AA6056-T6 were peened in an area of 20 mm × 20 mm. The residual stress profiles were determined using the measurement system 'Prism' (Stresstech) based on the

incremental hole drilling technique. The system is equipped with an optical electronic speckle pattern interferometer (ESPI) system that provides high-quality full-field displacement data for accurate residual stress calculation. This hole-drilling measurement technique has been described in detail by Steinzig and Ponslet.[49]

Two LSP treatments were investigated: one of them with only one overlap and the other with three overlaps, meaning that each spot is peened three times. The residual stress results are shown in Figure 7. No significant difference between the LSP treatments with only one and three overlap(s) was observed. However, there a noticeable difference between the residual stresses obtained in the longitudinal direction (σ_{xx}) and the transverse direction (σ_{yy}). The nonequibiaxiality in residual stress profiles could be attributed to the LSP treatment sequence and/or material texture, as observed for the LSP treatment of other high-strength Al-alloys as well.[50,51] Close to the specimen's surface, the absolute value of compressive residual stresses in the longitudinal direction is approximately 250 MPa, which refers to approximately 70% of the yield strength of the base material (approximately 350 MPa).[40] Chupakhin et al. have investigated the effect of elastoplastic material behaviour in determining residual stress profiles using hole-drilling techniques; they have proposed a correction methodology for the calculated residual stresses due to plastic deformation, which might occur during stress relaxation if residual stresses are close to the yield strength of the material.[52,53] However, if the absolute value of residual stresses does not exceed 80% of the material yield strength, it was shown that the error in the determination of residual stresses is less than 10%.[53] Consequently, it can be assumed that Figure 7 displays reasonable quantitative results regarding the determined depth that can resolve the residual stresses. The results indicate that deep compressive residual stresses in 6.2-mm-thick AA6056 specimens up to a depth of 2 mm can be generated via LSP. The zero-depth of the compressive residual stress profile of approximately 2 mm is significantly higher than the crack depth of 1.2 mm. Therefore, the investigated LSP treatment should reduce the resulting stress concentration at the crack tip. As the two LSP treatments resulted in comparable residual stress profiles, only one layer of LSP treatment was applied to the specimen's surfaces of precracked fatigue specimens to investigate the recovering effect of LSP on the fatigue life in the following section.

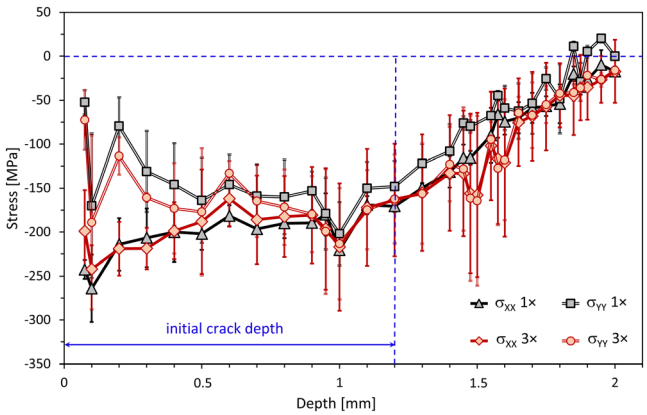

FIGURE 7 Residual stress profiles determined via hole drilling for two different LSP treatments with one and three overlap(s) of the base material. Average values with standard deviations from three measurements on flat base material specimens are shown. A spot size of 1 mm × 1 mm and the energy of 5 J were used as LSP process parameters [Colour figure can be viewed at wileyonlinelibrary.com]

3.3 | Retardation of surface fatigue cracks in laser beam-welded AA6056 through LSP

To quantify the effect of LSP, the following approach was followed to guarantee comparable testing conditions. The specimens with 1.2-mm deep naturally initiated fatigue cracks have been grouped into two batches. The specimens of the first batch have been tested at different stress levels to construct the S–N curve in the precracked condition. The second batch was first subjected to LSP and then tested at different stress levels to obtain the S–N curve in the cracked + LSP condition. The achieved S–N curves for different testing conditions, including the as-welded condition, are displayed in Figure 8.

As expected, the fatigue performance of specimens with the introduced initial fatigue cracks significantly reduced. The endurance limit gets reduced from approximately 85 MPa in the as-welded condition to approximately 70 MPa for the specimens with an initial crack with a depth of 1.2 mm. The applied LSP treatment to specimens containing a fatigue crack with a depth of 1.2 mm significantly improved fatigue behaviour. The observed fatigue life is comparable with the fatigue life of the specimens tested in the as-welded condition, where the endurance limit is even higher at approximately 100 MPa. So, the compressive residual stress field around the fatigue crack retards its subsequent propagation significantly.

Some comments should be made about the results of fatigue testing and their interpretation. The S–N approach for the LSP effect evaluation enables us to estimate the influence of fatigue cracks on allowable stress magnitudes. In this context, the fatigue limit at 10^7 cycles might be regarded as an allowable stress level. It can be

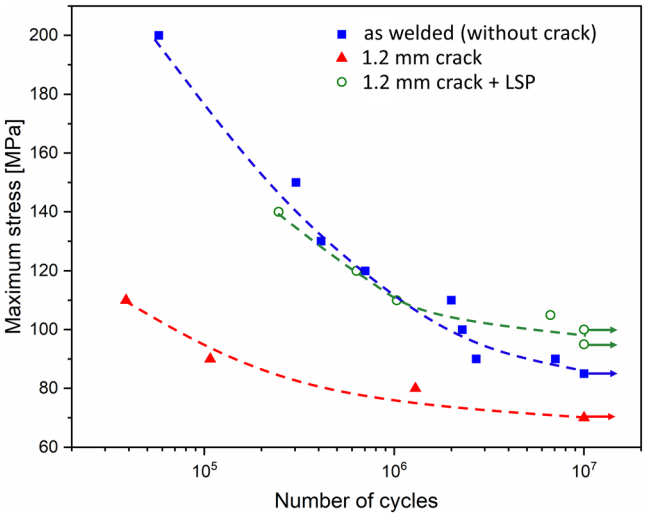

FIGURE 8 Fatigue test results of laser beam-welded specimens (as welded), laser beam-welded specimens with initial fatigue cracks (1.2-mm crack), as well as laser beam-welded specimens with initial fatigue cracks and the subsequent LSP treatment (1.2-mm crack + LSP) [Colour figure can be viewed at wileyonlinelibrary.com]

seen from Figure 8 that a surface crack with a depth of 1.2 mm degrades the load-bearing capacity of the welded joint. This reduction can be characterized by the fatigue limit drop from 85 to 70 MPa. In other words, the applied external loads should be decreased by around 20% to operate the welded part in the safe regime with the present fatigue cracks in a weld area. This value is a function of the crack depth, and the degradation is more severe for deeper cracks.

The introduction of compressive residual stresses at the crack tip leads to crack growth retardation and even crack arrest, as shown in Figure 8. Moreover, the stresses required for the 1.2-mm deep crack to grow further in the residual stress field are at least 100 MPa, which is even higher than the fatigue limit in the intact as-welded condition. This result points out that despite the detected crack, the allowable stress levels are at least equal to the intact fatigue limit. For practical applications, it would imply that LSP treatment leads to complete recovery of the load-bearing capacity of a component. The application of LSP treatment allows the recovery of the safe operation condition for the cracked component without any decrease in the applicable stress magnitudes. This, in turn, has major advantages regarding maintenance and replacement costs.

The results of fatigue testing indicate that the effect of LSP treatment depends on the applied stress level and consequently on the fatigue regime in which the material will be operated. Figure 8 shows that the impact of LSP is more pronounced in the region of a high number of cycles between 10^6 and 10^8—that is, when the crack approaches the threshold condition, it is normally referred to as the fatigue limit.[54] A more detailed overview of the theoretical background of the stages of the fatigue life and their definition can be found elsewhere.[55,56] It is important to note that the fatigue limit of 100–105 MPa for the cracked and LSP-treated specimens corresponds to the threshold stress, below which the crack ceases to propagate. In other words, the residual stress field at the crack tip reduces the stress intensity to a level that is not sufficient to initiate its further propagation. Thus, it might be concluded that the improvement of the fatigue limit in the LSP field could be attributed to the increased crack propagation threshold.

In the region between 10^5 and 10^6 loading cycles, LSP treatment results in a comparable lifetime as the initial S–N curve for the welded uncracked joint. The life prolongation in this region relies fully on the crack growth rate reduction in the LSP field. Because the LSP-treated specimens have been precracked, the entire fatigue life in this region can be attributed to the crack growth stage. Lower stress intensities at the crack tip growing through the LSP field yields the prolongation of the crack propagation stage and the fatigue life.

In Figure 9, the fractured surfaces of the two specimens with an initial surface fatigue crack of approximately 1.2 mm without and with LSP treatment and tested at 110 MPa are shown. The specimen, whose fractured surfaces are shown in Figure 9A,C, was without LSP treatment and experienced only 3.86×10^4 loading cycles until failure. Its fractured surfaces are similar to the specimen tested at the same stress level without an initial surface fatigue crack, as shown in Figure 6B. The aspect ratio of the ellipse that shape is partially close to the boundary between the stable and unstable fatigue crack growth is approximately 10:3. A stable fatigue crack growth can be seen in 33% of the total crack area—it is more or less comparable with 37% in case of the specimen without an initial surface fatigue crack represented in Figure 6B. The difference between the aspect ratios of the semielliptical cracks (2:1 in Figure 6B and 10:3 in Figure 9A for the specimen without an initial surface fatigue crack and for the specimen with an initial surface fatigue crack introduced under slightly different test conditions, respectively) can be attributed to the heterogeneous microstructure in the weld. As can be seen in Figure 6B, the crack initiation area is not located in the centre of the specimen surface. In case of the specimen in Figure 9A, the crack initiation site is located close to the centre of the specimen surface. On the SEM image of the fractured surface (Figure 9C), it was possible to identify the boundary of the introduced initial surface crack—this is marked with an ellipse with an aspect ratio of

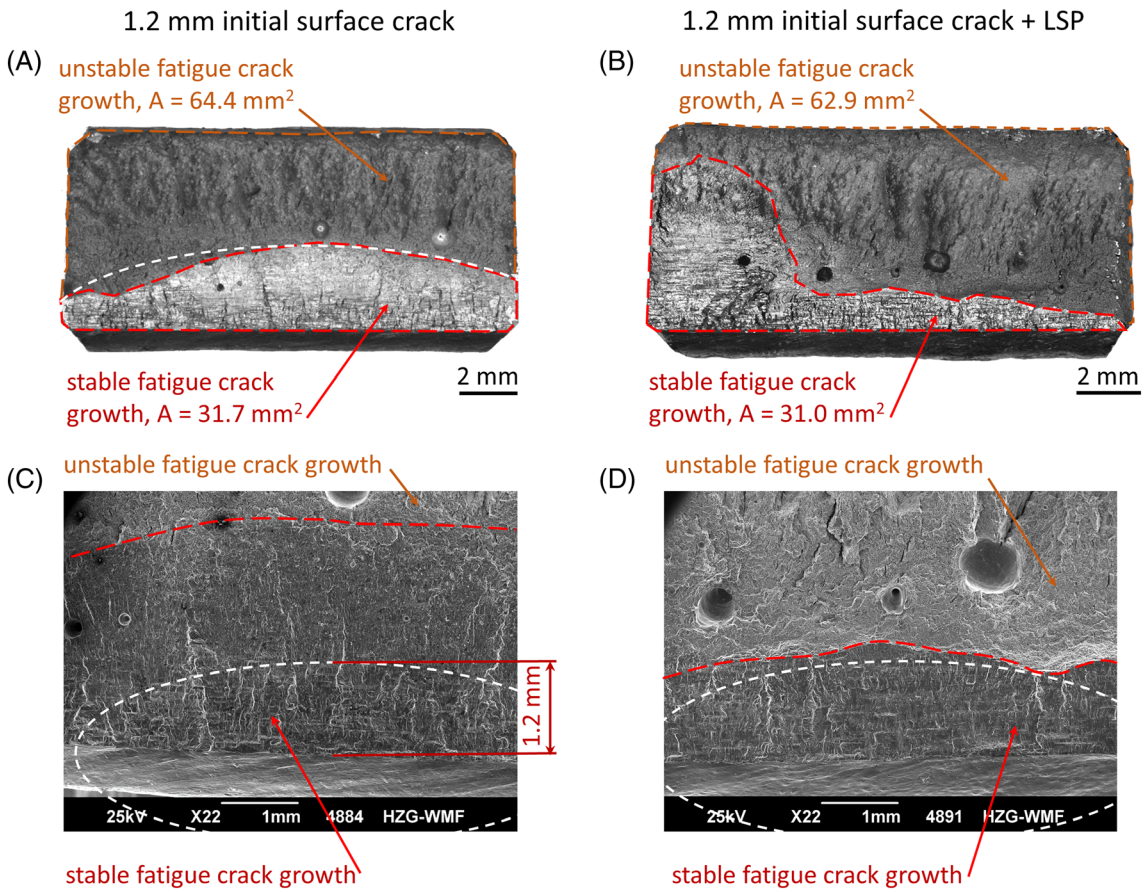

FIGURE 9 Micrographs of the fractured surface of (A) the specimen with an initial surface fatigue crack of 1.2 mm in depth that experienced 3.86×10^4 loading cycles and (B) the specimen with an initial fatigue crack of 1.2 mm in depth and LSP treatment that experienced 1.03×10^6 loading cycles. SEM images of the fractured surface of (C) the specimen in Figure 9A and (D) the specimen in Figure 9B. In both cases, the fatigue test was conducted at 110 MPa [Colour figure can be viewed at wileyonlinelibrary.com]

approximately 10:3. The boundary between the stable and unstable fatigue crack growth is also visible (indicated with a dashed red line). The depth of the initial semielliptical surface fatigue crack is approximately 1.2 mm. Observing the fractured surfaces of the specimens represented in Figures 6B and 9A, it can be concluded that the introduction of an initial surface fatigue crack does not have any significant influence on the appearance of the fractured surface after the failure of the specimen in the fatigue test.

Compared with the specimen with an initial surface fatigue crack without LSP treatment (Figure 9A,C), the LSP-treated specimen with an initial surface fatigue crack (Figure 9B,D) tested at the same stress level experienced a significantly higher number of loading cycles until failure (1.03×10^6). In comparison with the specimen without LSP treatment (Figure 9C), the area with an initial fatigue crack cannot be clearly identified in the SEM image of the fractured surface of the LSP-treated specimen (Figure 9D). The ellipse with an aspect ratio of 10:3 is depicted to show the probable area of the introduced fatigue crack. It can be seen that owing to the presence of compressive residual stresses, the growth of further fatigue cracks in the thickness direction was hindered (Figure 9B). The further fatigue crack growth took place from the left corner of the fractured surface to the thickness direction. This untypical crack growth took place because of the higher compressive residual stresses in the central region of the upper surface compared with a lower level of compressive residual stresses in the edge region of the upper surface.

When analysing the stereomicroscope images as well as the SEM images of fractured surfaces, it was not possible to specify the depth of affected area by the residual stresses. As the areas for stable crack growth for the specimen without LSP treatment (33%) and the LSP-treated specimen (33%) are comparable (Figure 9A,B), the effect of LSP could be only attributed to the retardation of the fatigue crack growth. However, in comparison with the propagation of long through-the-thickness fatigue cracks, where crack closure is the main mechanism,[30,33,57] any clear indications on crack closure could not be observed

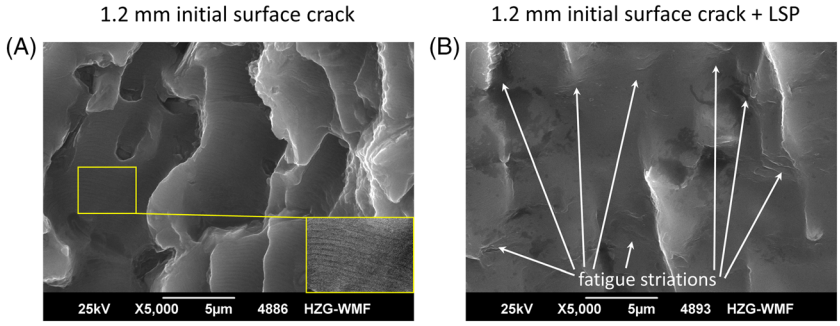

FIGURE 10 SEM images with a higher magnification of the fractured surface of (A) the specimen with an initial surface fatigue crack of 1.2 mm in depth that experienced 3.86×10^4 loading cycles and (B) the specimen with an initial fatigue crack of 1.2 mm in depth and the LSP treatment that experienced 1.03×10^6 loading cycles. In both cases, the fatigue test was conducted at 110 MPa [Colour figure can be viewed at wileyonlinelibrary.com]

in the fractured surfaces of the LSP-treated specimens investigated in the current study. When analysing details of the SEM-images of fractured surfaces (areas with a stable fatigue crack growth close to an initial fatigue crack), the specimen without LSP treatment shows very fine fatigue lines and fatigue striations within fatigue crack paths (see Figure 10A). In case of the LSP-treated specimen, these characteristics of the fatigue fracture appear occasionally only at several places, as indicated with white arrows in Figure 10B. This means that in case of the LSP-treated specimen, the significantly lower fatigue crack growth rate leads to the formation of very smooth fracture paths and reduction of height differences between all neighbouring fracture paths. The influence of LSP-induced residual stresses on the striation spacing has extensively been studied and reported by Hatamleh et al.[47] The authors have observed a smaller fatigue striations spacing for LSP-treated specimens in comparison with the specimens without LSP treatment. This is in good agreement with the results in the current study. The fatigue crack paths of the specimen without LSP treatment represents a block-like structure comprising fracture paths, fatigue lines and fatigue striations (Figure 10A)—this is typical for aluminium alloys.[58] The influence of LSP leading to the generation of compressive residual stresses suppresses the formation of this block-like structure (Figure 10B).

4 | CONCLUSIONS

In this study, the effect of LSP-induced residual stresses on the recovery of the fatigue life of precracked laser beam-welded AA6056 butt joints under uniaxial loading was investigated. Based on the obtained results, the following conclusions are drawn.

1 The crack tip diffraction using the ultrasonic-phased array system investigated in this study was proven as a promising approach to monitor fatigue crack growth during fatigue tests. The ultrasonic technique was calibrated on the introduced notches in the specimens using electro discharge machining. The inspection technique and its implementation have allowed us to measure the crack length with sufficient accuracy for relatively short cracks with a depth of 0.5–2.0 mm.
2 The initiating and growth of fatigue cracks in welded specimens during the fatigue test was possible to monitor based on a change in the resonant frequency. A good match between the frequency-based crack depth measurements and the ultrasonic testing has been found.
3 Surface fatigue cracks in laser beam-welded specimens significantly reduce their fatigue limit. A semielliptical fatigue crack with a depth of approximately 1.2 mm reduces the fatigue strength of the weld in the endurance limit by up to 20% in comparison with the specimens in the as-welded condition (without fatigue cracks).
4 Via the LSP treatment, it was possible to generate deep-compressive residual stresses in AA6056 6.2-mm sheet material up to a depth of approximately 2 mm. The fatigue performance of the precracked specimens after the LSP treatment was recovered; it was even better in comparison with the fatigue behaviour of as-welded specimens without fatigue cracks.

The results of the study propose LSP as an efficient technique to repair structural components where small cracks could be detected by nondestructive testing like ultrasonic testing. In this context, LSP treatment can be used to improve the fatigue behaviour of structural components where fatigue cracks can be initiated in critical areas such as welds. The results of this work demonstrate a high potential of LSP being applied as a prophylactic residual stress engineering approach to extend the fatigue life of critical structures in ageing aircrafts, where the fatigue cracks have not reached the detectable size. In this regard, LSP treatment could reduce the required safety margins (safety factors) of the fatigue critical component or structure, thereby reducing its weight. Future research should test the results in case of different aluminium alloys, different joint configurations and loading conditions.

ACKNOWLEDGEMENTS

The authors would like to thank Mr. Falk Dorn, Mr. Kai Erdmann, Mr. Christian Horstmann, Mr. Stefan Riekehr and Mr. René Dinse from the Helmholtz-Zentrum Geesthacht for their technical support and assistance in the experimental work.

NOMENCLATURE

A	uniform cross section
E	elastic modulus of the specimen
f_0	resonant (natural) frequency
k	system stiffness
k_m	stiffness of the machine
k_s	stiffness of the specimen
k_Σ	total stiffness of the system
L	length of the specimen
m	mass
R_F	load ratio
FOD	foreign object damage
FWHM	full width at half maximum
FZ	fusion zone
HAZ	heat-affected zone
LBW	laser beam welding
LSP	laser shock peening
SEM	scanning electron microscope

ORCID

Nikolai Kashaev https://orcid.org/0000-0001-5969-8560
Benjamin Klusemann https://orcid.org/0000-0002-8516-5087

REFERENCES

1. Rendings KH. Aluminium structures used in aerospace—status and prospects. *Mater Sci Forum*. 1997;242:11-24.
2. Pacchione M, Telgkamp J. Challenges of the metallic fuselage. In: *Proc. 25th International Congress of the Aeronautical Sciences*. Hamburg: International Council of the Aeronautical Sciences (ICAS); 2006.
3. Schmidt HJ, Schmidt-Brandecker B. Fatigue and damage tolerance behaviour of advanced structures in aeronautics. In: *Proc. 18th European Conference on Fracture - Fracture of Materials and Structures from Micro to Macro Scale*. Berlin: Deutscher Verband für Materialforschung und -prüfung e.V; 2010.
4. Miedlar PC, Berens AP, Gunderson A, Gallagher JP. *USAF Damage Tolerant Design Handbook: Guidelines for the Analysis and Design of Damage Tolerant Aircraft Structures*. Dayton: University of Dayton Research Institute; 2002.
5. Schijve J. Fatigue damage in aircraft structures, not wanted, but tolerated? *Int J Fatigue*. 2009;31:998-1011.
6. Tavares SMO, De Castro PMST. An overview of fatigue in aircraft structures. *Fatigue Fract Eng Mater Struct*. 2017;40(10):1510-1529.
7. Liebowitz H. *AGARDograph No. 176 on Fracture Mechanics of Aircraft Structures*. Neuilly-sur-Seine: North Atlantic Treaty Organization (NATO); 1974.
8. Pacchione M, Telgkamp J, Ohrloff N. Design of pressurized fuselage structures under consideration of damage tolerance requirements. In: *Berichtsband der 40. Tagung des DVM Arbeitskreises Bruchvorgänge - Zuverlässigkeit von Bauteilen durch bruchmechanische Bewertung: Regelwerke, Anwendung und Trends*. Berlin: Deutsche Verband für Materialforschung und -prüfung e.V. (DVM); 2008:335-353.
9. Zhang X, Boscolo M, Figueroa-Gordon D, Allegri G, Irving PE. Fail-safe design of integral metallic aircraft structures reinforced by bonded crack retarders. *Eng Fract Mech*. 2009;76(1):114-133.
10. Uz MV, Koçak M, Lemaitre F, Ehrström JC, Kempa S, Bron F. Improvement of damage tolerance of laser beam welded stiffened panels for airframes via local engineering. *Int J Fatigue*. 2009;31:916-926.
11. Lu J, Huber N, Kashaev N. Improving the fatigue performance of airframe structures by combining geometrical modifications and laser heating. *Fatigue Fract Eng Mater Struct*. 2018;41:1183-1195.
12. Schnubel D, Horstmann M, Ventzke V, et al. Retardation of fatigue crack growth in aircraft aluminium alloys via laser heating—experimental proof of concept. *Mater Sci Eng A*. 2012;A546:8-14.
13. Elber W. Fatigue crack closure under cyclic tension. *Eng Fract Mech*. 1970;2(1):37-45.
14. Novotny LG. Overstressing of pressure vessels to increase service life. In: *International Conference on Fatigue of Engineering Materials and Structures*. Vol.2 London: Institution of Mechanical Engineers; 1986:249-256.
15. Vardar Ö. Effect of single overload in FCP. *Eng Fract Mech*. 1988;30(3):329-335.
16. Miyagawa H, Nishitani H. Retardation of fatigue crack propagation due to additional holes or indentations in plate specimens. *Bull JSME*. 1985;28(244):2219-2223.
17. Song PS, Sheu GL. Retardation of fatigue crack propagation by indentation technique. *Int J Pres Ves Pip*. 2002;79:725-733.
18. Razavi SMJ, Ayatollahi MR, Amouzadi A, Berto F. Effects of different indentation methods on fatigue life extension of cracked specimens. *Fatigue Fract Eng Mater Struct*. 2018;41:287-299.
19. Buxbaum O, Huth H. Expansion of cracked fastener holes as a measure for extension of lifetime to repair. *Eng Fract Mech*. 1987;28(5–6):689-698.
20. Ball DL, Lowry DR. Experimental investigation of the effects of cold expansion of fastener holes. *Fatigue Fract Eng Mater Struct*. 1998;21:17-34.
21. Song PS, Shieh YL. Stop drilling procedure for fatigue life improvement. *Int J Fatigue*. 2004;26(12):1333-1339.
22. Ayatollahi MR, Razavi SMJ, Yahya MY. Mixed mode fatigue crack initiation and growth in a CT specimen repaired by stop hole technique. *Eng Fract Mech*. 2015;145:115-127.
23. Razavi SMJ, Ayatollahi MR, Sommitsch C, Moser C. Retardation of fatigue crack growth in high strength steel S690 using a

modified stop-hole technique. *Eng Fract Mech*. 2017;169:226-237.
24. Montross CS, Wei T, Ye L, Clark G, Mai YW. Laser shock processing and its effects on microstructure and properties of metal alloys: a review. *Int J Fatigue*. 2002;24:1021-1036.
25. McClung RC. A literature survey on the stability and significance of residual stresses during fatigue. *Fatigue Fract Eng Mater Struct*. 2007;30(3):173-205.
26. Sticchi M, Schnubel D, Kashaev N, Huber N. Review of residual stress modification techniques for extending the fatigue life of metallic aircraft components. *Appl Mech Rev*. 2015;67(1):010801.
27. Nalla RK, Altenberger I, Noster U, Liu GY, Scholtes B, Ritchie RO. On the influence of mechanical surface treatments—deep rolling and laser shock peening—on the fatigue behavior of Ti–6Al–4V at ambient and elevated temperatures. *Mater Sci Eng A*. 2003;A355:216-230.
28. Zhang XC, Zhang YK, Lu JZ, Xuan FZ, Wang ZD, Tu ST. Improvement of fatigue life of Ti–6Al–4V alloy by laser shock peening. *Mater Sci Eng A*. 2010;A527:3411-3415.
29. Hombergsmeier E, Holzinger V, Heckenberger UC. Fatigue crack retardation in LSP and SP treated aluminium specimens. *Adv Mater Res*. 2014;891-892:986-991.
30. Kashaev N, Ventzke V, Horstmann M, et al. Effects of laser shock peening on the microstructure and fatigue crack propagation behaviour of thin AA2024 specimens. *Int J Fatigue*. 2017;98:223-233.
31. Fomin F, Klusemann B, Kashaev N. Surface modification methods for fatigue properties improvement of laser-beam-welded Ti–6Al–4V butt joints. *Procedia Struct Integr*. 2018;13:273-278.
32. Pavan M, Furfari D, Ahmad B, Gharghouri MA, Fitzpatrick ME. Fatigue crack growth in a laser shock peened residual stress field. *Int J Fatigue*. 2019;123:157-167.
33. Hu Y, Cheng H, Yu J, Yao Z. An experimental study on crack closure induced by laser peening in pre-cracked aluminum alloy 2024-T351 and fatigue life extension. *Int J Fatigue*. 2020;130:105232.
34. Takahashi K, Kogishi Y, Shibuya N, Kumeno F. Effects of laser peening on the fatigue strength and defect tolerance of aluminium alloy. *Fatigue Fract Eng Mater Struct*. 2020;43:845-856.
35. Lin B, Lupton C, Spanrad S, Schofield J, Tong J. Fatigue crack growth in laser-shock-peened Ti–6Al–4V aerofoil specimens due to foreign object damage. *Int J Fatigue*. 2014;59:23-33.
36. Luo S, Nie X, Zhou L, Li Y, He W. High cycle fatigue performance in laser shock peened TC4 titanium alloys subjected to foreign object damage. *J Mater Eng Perform*. 2018;27:1466-1474.
37. Cini A, Irving PE. Development of fatigue cracks from mechanically machined scratches on 2024-T351 aluminium alloy—part I: experimentation and fractographic analysis. *Fatigue Fract Eng Mater Struct*. 2017;40:776-789.
38. Smyth NA, Toparli MB, Fitzpatrick ME, Irving PE. Recovery of fatigue life using laser peening on 2024-T351 aluminium sheet containing scratch damage: the role of residual stress. *Fatigue Fract Eng Mater Struct*. 2019;42:1161-1174.
39. Fabrègue D, Deschamps A, Suéry M. Influence of the silicon content on the mechanical properties of AA6xxx laser welds. *Mater Sci Eng A*. 2009;A506(1–2):157-164.
40. Pakdil M, Çam M, Koçak C, Erim S. Microstructural and mechanical characterization of laser beam welded AA6056 Al-alloy. *Mater Sci Eng A*. 2011;A528(24):7350-7356.
41. Vaidya WV, Staron P, Horstmann M. Fatigue crack propagation into the residual stress field along and perpendicular to laser beam butt-weld in aluminium alloy AA6056. *Fatigue Fract Eng Mater Struct*. 2012;35(5):399-411.
42. Kashaev N, Ventzke V, Çam M. Prospects of laser beam welding and friction stir welding processes for aluminum airframe structural applications. *J Manuf Proc*. 2018;36:571-600.
43. ASTM. *E466-07. Standard Practice for Conducting Force Controlled Constant Amplitude Axial Fatigue Tests of Metallic Materials*. ASTM International: West Conshohocken; 2007.
44. Jacques F, Moreau F, Ginzel E. Ultrasonic backscatter sizing using phased array—developments in tip diffraction flaw sizing. *Insight*. 2003;45(11):724-728.
45. Tabernig B, Pippan R. Determination of the length dependence of the threshold for fatigue crack propagation. *Eng Fract Mech*. 2002;69(8):899-907.
46. Lorenzino P, Navarro A. The variation of resonance frequency in fatigue tests as a tool for in-situ identification of crack initiation and propagation, and for the determination of cracked areas. *Int J Fatigue*. 2015;70:374-382.
47. Hatamleh O, Lyons J, Forman R. Laser and shot peening effects on fatigue crack growth in friction stir welded 7075-T7351 aluminum alloy joints. *Int J Fatigue*. 2007;29:421-434.
48. Chupakhin S, Klusemann B, Huber N, Kashaev N. Application of design of experiments for laser shock peening process optimization. *Int J Adv Manuf Technol*. 2019;102(5–8):1567-1581.
49. Steinzig M, Ponslet E. Residual stress measurement using the hole drilling method and laser speckle interferometry: part 1. *Exp Techniques*. 2003;27(3):43-46.
50. Toparli MB, Fitzpatrick ME. Effect of overlapping of peen spots on residual stresses in laser-peened aluminium sheets. *Metall Mater Trans A*. 2019;50:1109-1112.
51. Kallien Z, Keller S, Ventzke V, Kashaev N, Klusemann B. Effect of laser peening process parameters and sequences on residual stress profiles. *Metals*. 2019;9(6):655.
52. Chupakhin S, Kashaev N, Huber N. Effect of elasto-plastic material behaviour on determination of residual stress profiles using the hole drilling method. *J Strain Anal Eng Des*. 2016;51(8):572-581.
53. Chupakhin S, Kashaev N, Klusemann B, Huber N. Artificial neural network for correction of effects of plasticity in equibiaxial residual stress profiles measured by hole drilling. *J Strain Anal Eng Des*. 2017;52(3):137-151.
54. Murakami Y. *Metal Fatigue: Effects of Small Defects and Nonmetallic Inclusions*. 1st ed. Oxford: Elsevier Science Ltd; 2002.
55. Schijve J. *Fatigue of Structures and Materials*. 2nd ed. Delft: Springer; 2009.

56. Madia M, Zerbst U, Beier HT, Schork B. The IBESS model—elements, realisation and validation. *Eng Fract Mech*. 2018;198:171-208.
57. Keller S, Horstmann M, Kashaev N, Klusemann B. Crack closure mechanisms in residual stress fields generated by laser shock peening: a combined experimental-numerical approach. *Eng Fract Mech*. 2019;221:106630.
58. Webster A. Properties and microstructure of aluminium-copper-magnesium-lithium alloys. *Metall Trans A*. 1979;10:1913-1921.

How to cite this article: Kashaev N, Ushmaev D, Ventzke V, Klusemann B, Fomin F. On the application of laser shock peening for retardation of surface fatigue cracks in laser beam-welded AA6056. *Fatigue Fract Eng Mater Struct*. 2020;43:1500–1513. https://doi.org/10.1111/ffe.13226